

# Supporting Information for: Simulation of Self-Heating Process on the Nanoscale: a Multiscale Approach for Molecular Models of Nanocomposite Materials

Greta Donati,<sup>\*,†</sup> Antonio De Nicola,<sup>‡</sup> Gianmarco Munaò,<sup>¶</sup> Maksym Byshkin,<sup>§</sup>  
Luigi Vertuccio,<sup>||</sup> Liberata Guadagno,<sup>||</sup> Ronan Le Goff,<sup>⊥</sup> and Giuseppe Milano<sup>†</sup>

<sup>†</sup>*Department of Chemistry and Biology, University of Salerno, Via Giovanni Paolo II 132,  
84040 Fisciano (SA), Italy*

<sup>‡</sup>*Department of Organic Materials Science, Yamagata University, 4-3-16 Jonan Yonezawa,  
Yamagata-ken 992-8510, Japan*

<sup>¶</sup>*Department of Mathematical and Computer Sciences, Physical Sciences and Earth  
Sciences, University of Messina, Viale Stagno d'Alcontres 31, 98166 Messina, Italy*

<sup>§</sup>*Institute of Computational Science, Università della Svizzera Italiana, 6900 Lugano,  
Switzerland*

<sup>||</sup>*Department of Industrial Engineering, University of Salerno, Via Giovanni Paolo II 132,  
84084 Fisciano (SA), Italy*

<sup>⊥</sup>*IPC Technical Center - Centre Technique Industriel de la Plasturgie et des Composites,  
Bellignat, France*

E-mail: gdonati@unisa.it

# S1 Molecular Dynamics Simulations

## S1.1 The Hybrid Particle-Field Approach

In the framework of self-consistent field theory (SCF), the model systems are not represented by particles but by density fields and the inter-molecular interactions are evaluated as interactions with static external fields instead of particle-particle interactions. These field-based approaches allow for the simulation of materials on scales much larger than the ones particle-based. Recently, hybrid particle-field approach (hPF) method combining a microscopic molecular representation to density-based potential, has been introduced.<sup>1-3</sup> This technique has been proposed within a molecular dynamics framework (hPF-MD) and successfully validated and widely employed in many applications, giving excellent results and drastic reduction of the computational cost.<sup>4,5</sup> This approach, implemented in the OCCAM software<sup>6</sup> and employed in this work to simulate the aggregation of the CNTs in the polymer matrix, will be briefly described in this section. The main feature of hPF-MD approach is that non-bonded forces and potentials are replaced by the calculation of external potentials depending on the local density at position  $\mathbf{r}$ .<sup>4</sup> According to the SCF theory a multi-body problem such as the molecular motion can be reduced to the problem of deriving the partition function of a molecule in an external potential  $V(\mathbf{r})$ , and to obtain a convenient  $V(\mathbf{r})$  expression and its derivatives. The form of the density dependent interaction potential  $W$ , where each species is specified by the index  $K$ , takes the following form:

$$W[\{\phi_K(\mathbf{r})\}] = \int d\mathbf{r} \left( \frac{k_B T}{2} \sum_{KK'} \chi_{KK'} \phi_K(\mathbf{r}) \phi_{K'}(\mathbf{r}) + \frac{1}{2\kappa} \left( \sum_K \phi_K(\mathbf{r}) - \phi_0 \right)^2 \right) \quad (\text{S1})$$

where  $\phi_K(\mathbf{r})$  is the coarse-grained density of species  $K$  at position  $r$  and  $\chi_{KK'}$  are the mean field parameters for the interaction of a particle of type  $K$  with the density field due to the particles of type  $K'$ . The second term represents the incompressibility condition and  $\kappa$

is the compressibility acting against local density inhomogeneity, assumed to be sufficiently small, while  $\phi_0$  is the total number density of the system.<sup>6</sup> By using the so-called saddle point approximation, it can be shown that the external potential is given by:

$$V_K(\mathbf{r}) = \frac{\delta W[\phi_K(\mathbf{r})]}{\delta \phi_K(\mathbf{r})} = k_B T \sum_{K'} \chi_{KK'} \phi_{K'}(\mathbf{r}) + \frac{1}{\kappa} \left( \sum_K \phi_K(\mathbf{r}) - \phi_0 \right) \quad (\text{S2})$$

To connect the particle and field models for the proposed scheme, it is necessary to obtain a smooth coarse-grained density function directly from the particle positions. This function can be obtained by a mesh-based approach, that must be able to also give the density derivatives required to calculate the forces acting on the molecules. Further details on the derivation of the equation above and on the OCCAM code are given elsewhere.<sup>4-6</sup>

## S1.2 Mesh-based Approach for Density Function

A smooth coarse-grained density function ( $\phi(\mathbf{r})$ ) required for the MD-SCF scheme and derived directly from particle positions  $\Gamma$  is obtained from a mesh-based approach. Let us denote this procedure as:<sup>4</sup>

$$\bar{S}\{\hat{\phi}(\mathbf{r}; \Gamma)\} = \phi(\mathbf{r}) \quad (\text{S3})$$

Where  $S$  is a symbolic name of the mapping from the particle positions to the coarse-grained density. The potential energy at a given time during the simulation is the sum of both intramolecular interaction potentials (bond, angle and intramolecular non bonded) and density dependent mean field potential, where this one is obtained from the initial configuration of the system at the beginning of the simulation. During the simulation, the density is updated according to the updated particle positions in the simulation box, and from it a new value of the potential energy is calculated and then new forces.

In order to obtain the coarse-grained density, according to their position in the simulation box, the explicit particles are distributed in grid elements in which the simulation box is divided in the three dimensions. The density and its derivatives used for the calculation of the forces and potential energy due to particle-field interactions are defined on three-dimensional lattice points obeying the periodic boundary conditions. The values of the density function at position  $\mathbf{r}$  between lattice points are evaluated using linear interpolation of the values at neighbor latticed points.

In the implemented scheme the particle fractions are not assigned to the cell elements (lower order choice) but to the cell vertexes, according to a scheme shown in Figure S1 where a two-dimensional case is presented.

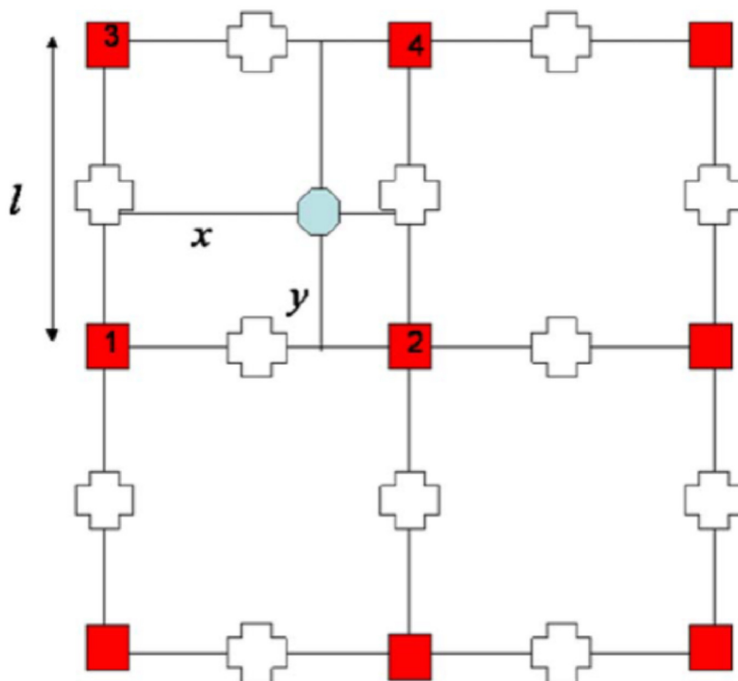


**Figure S1.** Geometry of particles fraction assignment in a two-dimensional case. This picture is taken from Ref. 4.

In particular, the fraction of a particle assigned to a given vertex is proportional to the area of a rectangle whose diagonal is the line connecting the particle position and the mesh point on the opposite site of the cell. For instance, a fraction  $x * y/l^2$  is assigned to the

mesh point 1.  $l$  is the length of a side of the cell. The three-dimensional case is just a simple extension where the particle fraction is a volume instead of an area. This approach allows to keep a more precise information on the initial particle position and at the same time the sensitivity to the particles configuration inside the cell element is higher since a fraction of the particle is assigned to the cell verteces according to the distance from them.<sup>4</sup> Instead, a particle assignment to the cell element (lower order choice), could not disentangle among different orientations of the particles inside the cell and a less accurate description and density function would be obtained. This picture advantages directly reflect in the Joule heating calculation accuracy since a more detailed map of the molecules positions is kept. Indeed, the local density on the verteces are employed for the calculation of local electrical conductivities, necessary for the evaluation of the Joule heat generation.

### **S1.3 Computational Details**

All the random conformations of CNT filled polymers are generated by using the Packmol software. The assembled systems both in monomer and linear polymer, starting from random configurations, are obtained by running hybrid particle-field dynamics with the OCCAM software package. In this way, the computational cost is importantly reduced. All the studied systems are treated at coarse grain level of theory and all the details of the coarse grain model and the details of the performed simulations are the same already successfully used in a previous work.<sup>7</sup> For all the simulated composite materials, the CNTs length is about 28 nm and the diameter is 1.4 nm, so the aspect ratio is about 20 in all cases, the cubic simulation box length is 113.12 nm, the grid length for the density field calculation is of about 2.1 nm, and a density update frequency was set to 300 time steps.

To obtain the assembled morphologies, for all the systems the NVT ensemble was employed keeping the temperature constant at 300 K using the Andersen thermostat with a collision frequency of  $20 \text{ ps}^{-1}$ . All the simulations were about 2  $\mu\text{s}$  long and a timestep of 0.03 ps was chosen.

To describe bonds between consecutive beads an harmonic potential was used:

$$V_{bond}(R) = \frac{1}{2}K_{bond}(R - R_{bond})^2 \quad (S4)$$

where an equilibrium distance set to 1.12 nm for CNTs and 1.4 nm for the polymer and a force constant  $K_{bond}$  of 10000 KJ/mol is used in both cases. The CNTs stiffness is taken into account by an harmonic potential depending on the cosine of angle among the beads where  $\theta$  is the angle between two successive bonds:

$$V_{angle}(\theta) = \frac{1}{2}K_{angle}\{\cos(\theta) - \cos(\theta_0)\}^2 \quad (S5)$$

where the equilibrium bond angle was set to  $\theta_0 = 180^\circ$  while the force constant  $K_{angle}$  was set to 8000 KJ/mol. Regarding non-bonded repulsive interactions between CNTs and polymer beads, the interaction parameter was set to:  $\chi_{KK'} \times RT = 12$  KJ/mol. All the systems and simulations details are resumed in Table S1, Table S2 and Table S3.

**Table S1.** Simulation details of nanocomposites molecules lengths and simulation box length.

No. beads of one CNT	No. beads of one polymer chain	No. beads of one monomer	Box length (nm)
25	25	1	113.12

**Table S2.** Composition details of all the simulated composite systems in polymer matrix.

Vol %	No. of CNTs	No. of polymer chains	Total no. of molecules	Total no. of beads	Simulated time ( $\mu$ s)
1	176	17424	17600	440000	2.8
2	352	17248	17600	440000	2.5
3	528	17072	17600	440000	2.5
4	704	16896	17600	440000	2.5
5	880	16720	17600	440000	0.5
6	1056	16544	17600	440000	1.3
7	1232	16368	17600	440000	1.3
8	1408	16192	17600	440000	0.5
9	1584	16016	17600	440000	0.5
10	1760	15840	17600	440000	1.7

**Table S3.** Composition details of all the simulated composite systems in monomer matrix.

Vol %	No. of CNTs	No. of monomers	Total no. of molecules	Total no. of beads	Simulated time ( $\mu$ s)
1	176	435600	435776	440000	11.4
2	352	431200	431552	440000	2.7
3	528	426800	427328	440000	1.8
4	704	422400	423104	440000	2.7
5	880	418000	418880	440000	2.8
6	1056	413600	414656	440000	1
7	1232	409200	410432	440000	1
8	1408	404800	406208	440000	1.4
9	1584	400400	401984	440000	2.3
10	1760	396000	397760	440000	1

## S2 Temperatures Time Evolution

In this Section we show for some of the analysed case studies the linear trend of temperature rise against the time found in all the simulations. In particular, for the random morphology and assembled morphology in monomer and polymer we show in Figure S2 and Figure S3 the temporal evolution of the temperature, obtained by averaging over all the local temperatures, when an external voltage of 30 or 40 V is applied, respectively. These are the simulations that have been compared with experimental data from.<sup>8</sup> As observed from the heating rates, the temperatures rise more in the assembled morphologies with respect to the random one. Moreover, in all cases higher temperatures are reached when larger voltage are applied.

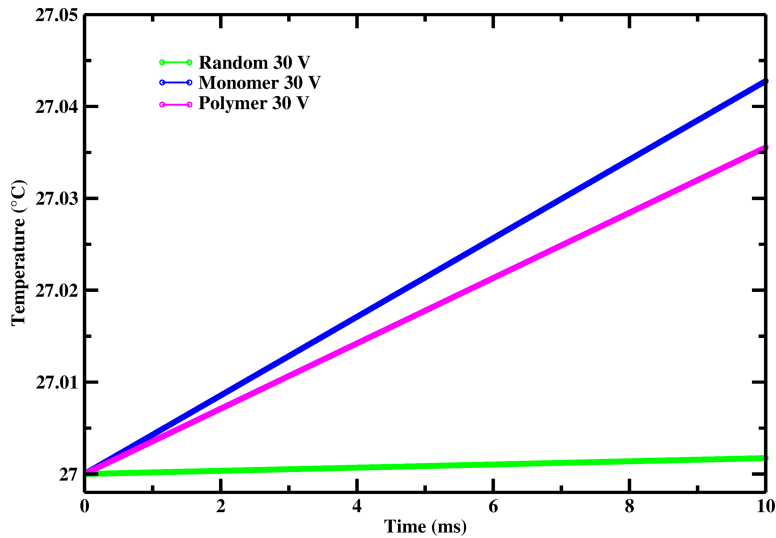


**Figure S2.** Temperature time evolution for random and assembled morphologies after the application of an external voltage of 30 V.

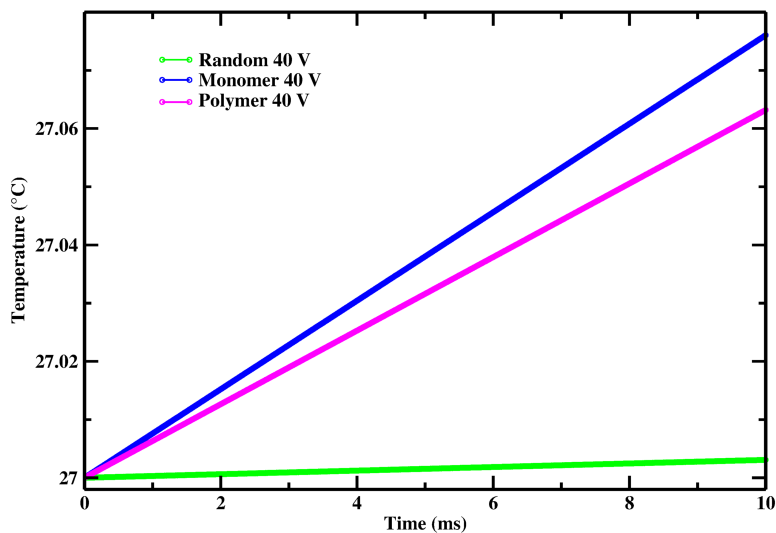


**Figure S3.** Temperature time evolution for random and assembled morphologies after the application of an external voltage of 40 V.

### S3 Energy Conservation in Heat Diffusion Equation

The energy conservation requirement for the heat transfer process states that the rate at which thermal energy enters the control volume plus the rate of energy generation (if any) is equal to the rate at which thermal energy leaves the control volume plus the rate of energy storage inside the control volume. For an unsteady state case of heat diffusion, i.e. the

temperature changes with time, the rate of energy storage inside the control volume is:

$$\rho c l_\alpha \frac{T_i(t+1) - T_i(t)}{\Delta t} \quad (\text{S6})$$

where  $\rho$  is the mass density in  $\text{g}/\text{nm}^3$ ,  $c$  is the specific heat in  $\text{J}/\text{gK}$ ,  $T_i$  is the temperature in  $\text{K}$  in the grid vertex  $i$  at time  $t$  or  $t+1$ ,  $\Delta t$  is the time step,  $l_\alpha$  is the grid length in the  $\alpha$  direction. This term is calculated for the three directions, and is added to the energy balance expression where the rate of heat entering a cell element (in our case a vertex) has to be equal to the rate of heat exiting from it when there is not a heat source, plus such term, measured in  $\text{W}/\text{nm}^3$ :

$$-k \frac{T_i(t) - T_{i-1}(t)}{l_\alpha} = -k \frac{T_{i+1}(t) - T_i(t)}{l_\alpha} + \rho c l_\alpha \frac{T_i(t+1) - T_i(t)}{\Delta t} \quad (\text{S7})$$

where  $k$  is the thermal conductivity ( $\text{W}/\text{nmK}$ ). All but one temperatures are evaluated at time  $t$  beside only one calculated at time  $i+1$ .

In Figure S4, the sum of all these contributions to the energy balance is presented. Such sum has to be zero on each vertex of the grid and the sum on all the verteces is shown. This requirement is successfully tested on each case study presented in the paper, confirming the correct implementation of the code for the heat diffusion equation, in agreement with the physical requirement of the energy conservation.

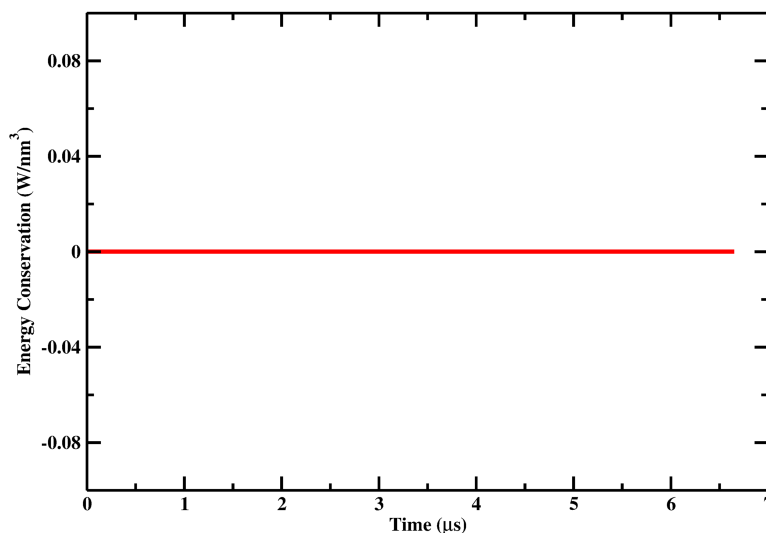


**Figure S4.** Sum of all the contributions to the heat transfer process. Rates of thermal energy entering and leaving a grid element are all considered and summed for all the vertices of the grid.

## References

- (1) Daoulas, K. C.; Muller, M. *J. Chem. Phys.* **2006**, *125*, 184904.
- (2) Daoulas, K. C.; Muller, M.; de Pablo, J. J.; Nealey, P. F.; Smith, G. D. *Soft Matter* **2006**, *2*, 573–583.
- (3) Daoulas, K. C.; Cavallo, A.; Shenhar, R.; Muller, M. *Soft Matter* **2009**, *5*, 4499–4509.
- (4) Milano, G.; Kawakatsu, T. *J. Chem. Phys.* **2009**, *130*, 214106.
- (5) Milano, G.; Kawakatsu, T. *J. Chem. Phys.* **2010**, *133*, 214102.
- (6) Zhao, Y.; Nicola, A. D.; Kawakatsu, T.; Milano, G. *J. Comput. Chem.* **2012**, *33*, 868–880.
- (7) Zhao, Y.; Byshkin, M.; Cong, Y.; Kawakatsu, T.; Guadagno, L.; Nicola, A. D.; Yu, N.; Milano, G.; Dong, B. *Nanoscale* **2016**, *8*, 15538.
- (8) Jeong, Y. G.; Jeon, G. W. *ACS Appl. Mater. Interfaces* **2013**, *5*, 6527.